Effects of selenization time and temperature on the growth of Cu$_2$ZnSnSe$_4$ thin films on a metal substrate for flexible solar cells

A.V. Stanchik[a], V.F. Gremenok[a], R. Juskenas[b], I.I. Tyukhov[c,*], M.S. Tivanov[d], Ch. Fettkenhauer[e], V.V. Shvartsman[e], R. Giraitis[b], U. Hagemann[f], D.C. Lupascu[e]

[a] *Scientific and Practical Materials Research Center, National Academy of Sciences of Belarus, 19, P. Brovki St., 220072 Minsk, Belarus*
[b] *State Research Institute Center for Physical Sciences and Technology, 231, Sauletekio Av., Vilnius, Lithuania*
[c] *San Jose State University, Department of Mechanical Engineering, One Washington Square, San Jose, CA 95192-0087, USA*
[d] *Belarusian State University, 4, Nezavisimosti Av., 220030 Minsk, Belarus*
[e] *Institute for Materials Science and Center for Nanointegration Duisburg-Essen, University of Duisburg-Essen, 15, Universitats St., 45141 Essen, Germany*
[f] *Center for Nanointegration Duisburg-Essen (CENIDE), Interdisciplinary Center for Analytics on the Nanoscale (ICAN), University of Duisburg-Essen, 199, Carl-Benz-Strasse, 47057 Duisburg, Germany*

ARTICLE INFO

ABSTRACT

Thin film Cu$_2$ZnSnSe$_4$ (CZTSe) solar cells can be grown on flexible and lightweight metal substrates allowing their direct integration on bendable surfaces and where the weight of solar cell is an important criterion. Flexible substrates make it possible to use the roll-to-roll technology of solar cells, which leads to an additional reduction in the cost of production and final cost of solar cells. The CZTSe thin films were fabricated by selenization of electrodeposited metallic precursors onto tantalum (Ta) flexible substrates at different temperature and time. The results of the effect of selenization temperature and time on the morphology, structural, and optical property of the CZTSe films are presented in this work. It was found that the morphology of the CZTSe thin films depend on their elemental composition and time of selenization. Experimental data indicate that composition of the CZTSe films selenized within 10 and 20 min at 560 °C have the CZTSe basic phase and secondary phases (CuSe, SnSe and ZnSe). In contrast, the increase in selenization temperature and/or time leads to disappearing of the secondary phases (CuSe, SnSe) and better crystallization of the CZTSe films. It was found that films selenized at 560 and 580 °C within the same time have similar characteristics. Depending on selenization time and temperature of the CZTSe, thin films exhibited a shift in band gap from 1.16 to 1.19 and to 1.22 eV, respectively. The change of band gap of the CZTSe thin films is associated with changes of elemental and phase compositions, and thickness of the film. These results showed that the received CZTSe films on Ta foil can be used for fabrication of thin film solar cells.

1. Introduction

Currently, silicon (Si), copper indium gallium selenide (CIGSe) and cadmium-telluride (CdTe) are leading solar cell technologies due to their high efficiency (Green et al., 2017). However, the silicon technology is expensive (Luck, 2014). The CdTe and CIGSe and technologies suffer from issues of toxicity and low abundance of raw materials, which are predicted to severely limit the manufacturing, mass deployment, and economic sustainability of solar cells production (Moskowitz and Fthenakis, 1990; Green, 2009). The kesterite Cu$_2$ZnSnSe$_4$ (CZTSe) is promising absorber material for cost effective thin film solar cells due to direct optical band gap (~1.0 eV), high absorption coefficient (10^{-4} cm^{-1}), p-type conductivity, low thermal conductivity, and this

material is made of abundant and low-toxicity elements. The highest conversion efficiency of CZTSe solar cells on glass substrates is 11.6% (Lee et al., 2014; Das et al., 2016).

In recent years, few attempts have been made to deposit CZTSe on metal flexible substrates because of the potential to reduce production costs (Kaigawa et al., 2015; Kessler and Rudmann, 2004; Khalil et al., 2017; Lopez-Marino et al., 2016; Stanchik et al., 2018). Flexible modules offer several advantages for their manufacturing and applications compared to modules on glass substrates (Bojic et al., 2016; Jayawardena et al., 2013; Kesler et al., 2005; Otte et al., 2006; Pagliaro et al., 2008). Solar cells on flexible substrates are very thin, light-weight and they can be applied on bendable surfaces, which makes them also more suitable in use. Another advantage of flexible substrates is the

---

potential to use roll-to-roll technology for the production of thin films which lead to much faster payback of solar cells because of high-throughput processing and low cost of the overall system (Kessler and Rudmann, 2004). The highest conversion efficiency of CZTSe solar cells on flexible metal substrates is reported to be 6.1%, where the CZTSe layer was produced by two-stage process (Lopez-Marino et al., 2016). If the two-stage film production process uses a combination of vacuum and non-vacuum methods, the production costs can be additionally reduced (Abermann, 2013). Recently, various non-vacuum methods have been applied to form precursors in the first step of the CZTSe films growth. Among these methods, electrochemical deposition is promising because of its low cost, easy to control, efficient use of materials, high-throughput and nontoxic process (Aksu et al., 2009; Deligianni et al., 2011; Guo et al., 2014; Klochko et al., 2014). In the second step annealing of the precursor in Se containing atmosphere is conducted (selenization). Phase CZTSe may form at temperatures 300 °C but higher temperatures should be applied for a sufficient CZTSe crystallization and conversion of binary and ternary phases into the main CZTSe phase (Fella et al., 2013). Preliminary annealing (pre-annealing) of metallic precursors can be applied before selenization in order to achieve homogenization of metal layer, especially if the stacked layer deposition was employed (Jiang et al., 2013). According to Kim et al. (2016) this step improves the final CZTSe solar cell performance. However, less study is devoted to preparation of the CZTSe films by the three-step method than by the two-step method, and the existing literature mainly focus on the CZTS thin films. Nevertheless, some of the problems need further investigation to increase performance CZTSe-based solar cells on metal flexible and/or glass substrates. In particular, the growing of single-phase CZTSe films without Zn-Se and more detrimental Sn-Se, Cu-Se and Cu_2SnSe_3 secondary phases is not an entirely resolved problem (Amiri and Postnikov, 2012; Fairbrother et al., 2014; Hartnauer et al., 2016; Just et al., 2016; Temgoua et al., 2014), and the effect of metal substrates on the properties of thin films is not uniquely. The comprehensive study about the effects of selenization time and temperature on both the properties of CZTSe film and the solar cell the properties is still limited (Fairbrother et al., 2014; Fella et al., 2012; Mangan et al., 2015; Marquez-Prieto et al., 2016; Yao et al., 2017). In this work, we have systematically investigated the influence of selenization time and temperature on the structure, morphology, secondary phase's formation and optical properties of CZTSe films obtained onto a flexible Ta substrate by the three-step method.

2. Experimental

2.1. Synthesis of CZTSe thin films

The CZTSe thin films were fabricated by the three-step process (precursor deposition, pre-annealing and selenization). The metal Cu/Sn/Zn precursors were sequentially electrochemically deposited on a Ta foil using metal plates with 99.99% purity (Gremenok et al., 2016; Gremenok et al., 2017). Preliminary annealing of the deposited metal precursors was conducted in 95% Ar + 5% H_2 atmosphere at a temperature of 350 °C for 30 min, after which the precursors were cooled to room temperature. The pre-annealed precursors were converted into the CZTSe films by selenization in a tubular quartz furnace. The pre-annealed precursors and 13 mg of selenium powder were loaded into a quartz box, and inserted into the furnace. The selenization was performed at temperature 560 °C, with a different duration time of 10, 20, 30 min, and at temperature 580 °C, with a duration time of 30 min.

2.2. Characterization

SEM characterization of CZTSe films surface morphology, focused ion beam (FIB) prepared cross-sections and EDX analysis of the films were carried out in a dual beam system FE-SEM-FIB Helios Nanolab 650 (FEI Company) equipped with an x-ray spectrometer X-Max (Oxford Instruments). The phase composition and crystalline structure of the materials were studied using a PANalytical diffractometer operating with CuK_α radiation. Analysis of the phase composition was performed with the use of the database of the Crystallography Open Database (COD). For study the lattice parameters of films we used the Rietveld analysis (Rietveld, 1969), implemented in the «Material Analysis Using Diffraction» (MAUD) software package (Lutterotti et al., 1999).

Time-of-Flight Secondary Ion Mass Spectrometry (TOF-SIMS) depth profiles were performed on a TOF.SIMS 5-100 from IONTOF equipped with a Bi primary ion gun and a Xe sputter source. Depth profiles were performed in the interlaced mode with Xe^+ sputtering incident with an impact energy of 2 keV. The scanning area was 300×300 μm^2. For the analysis beam Bi_1^+ primary ions are used at ion energies of 30 keV in the spectrometry mode with the positive polarity of the analyzer. The lateral resolution was 3–10 µm. The analyzed area defined by rastering the Bi ion beam was 100×100 μm^2. The Bi_1^+ is chosen for the analysis beam in order to maximize the mass resolution.

The spectral dependences of reflectance of the CZTSe films were carried out using a spectrophotometer MC122. Measurements were carried out in the spectral range from 300 to 1100 nm with spectral resolution of 3 nm (angle for reflected radiation measurements of 20°).

3. Results and discussion

In this work three series of Cu-Sn-Zn precursors, named A, B and C, were prepared. The precursors A and C series were Zn-rich, and the precursors B series were close to the stoichiometric composition.

The elemental composition of CZTSe thin films depending on time and temperature of selenization is depicted in Table 1. The ratios of Cu/(Zn + Sn) and Sn content decrease while ration Zn/Sn increases with the increasing the annealing time. The changes in the elemental concentration was due to the formation of SnSe, which has a much higher vapor pressure than Sn (Redinger and Siebentritt, 2010). Moreover, the amount of Se and Se/metal ratio of CZTSe film series A also gradually increases, indicating that sufficient selenization is achieved. However, the amount of Se and Se/metal ratios of CZTSe film series B initially increases then decreases with the annealing time probably due to

Table 1
The elemental composition and corresponding Zn/Sn, Cu/(Zn + Sn), Se/metal ratios of the CZTSe thin films depending on time and temperature of selenization.

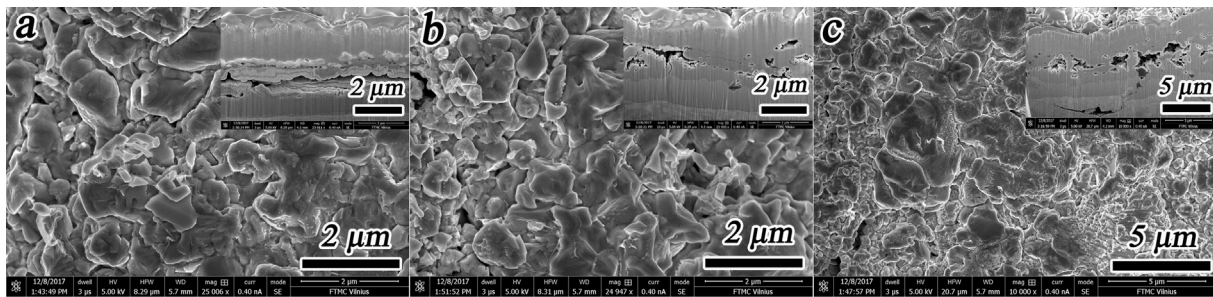| Series	Temperature of selenization, °C	Time of selenization, min	Atomic percent				Ratio		
			Cu	Zn	Sn	Se	Zn/Sn	Cu/(Zn + Sn)	Se/metal
A	560	10	27.55	15.5	11.82	45.13	1.31	1.01	0.82
		20	25.09	17.21	11.44	46.26	1.50	0.88	0.86
		30	24.61	17.39	11.13	46.87	1.56	0.86	0.88
B		10	23.36	12.8	11.54	52.30	1.11	0.96	1.10
		20	21.25	13.8	12.27	52.68	1.12	0.82	1.11
		30	18.4	21.21	8.8	51.59	2.41	0.61	1.07
C	580	30	22.09	18.53	10.83	48.54	1.71	0.75	0.94

Fig. 1. Top view SEM images of CZTSe films series A obtained at selenization temperature of 560 °C and selenization time of 10 (*a*), 20 (*b*) and 30 (*c*) min. Inset to (*a–c*) shows the typical cross-sectional image of CZTSe films series A.

higher evaporation of tin selenide. Sn loss is relatively higher for CZTSe films series B.

Comparing the elemental composition of CZTSe films series A and C obtained at temperature 560 and 580 °C within 30 min, a slight difference of the Zn/Sn and Cu/(Zn + Sn) ratios is observed. In both series, the CZTSe films are Cu-poor and Zn-rich, which corresponds to the optimal composition for solar cells with increased efficiency. The high-efficiency CZTSe-based solar cells have a composition ratio of 1.1–1.2 for Zn/Sn and 0.8–0.9 for Cu/(Zn + Sn) (Das et al., 2016). However, in our cases the Zn/Sn ratio is greater than 1.2.

Top view SEM images of CZTSe thin films of different selenization time are shown on Figs. 1 and 2. From the images, it can be seen that different morphologies are formed depending on the elemental composition (Xie et al., 2015; Kondrotas et al., 2015).

In both cases, the CZTSe films after 10 min selenization are crack-free and consist of two types of crystals. The small crystals have a size of about 500 nm and the size of large crystals is about one micron. The further increase of selenization time to 20 min has no significant impact on the morphology of CZTSe films series A with two types of crystals still visible (Fig. 1b). The SEM images of CZTSe films series B (Fig. 2b) clearly show the formation of small crystals with Zn-rich composition and large crystals that are identified as SnSe crystals. As can be seen from Figs. 1 and 2*c*, the CZTSe thin film after 30 min selenization shows a denser surface morphology. As the selenization time increases, the size of large grains are enlarged (Figs. 1 and 2*c*). The size of crystals on surfaces CZTSe films series A and B is about 1.5 and 1.7–3.5 μm, respectively. However, some small white grains, which have been previously attributed to ZnSe (Salome et al., 2014), still present on the surface of the films. When the Zn/Sn ratio are 2.41 (the CZTSe films series B), small white particles almost cover the whole film surface, and the size of grain decreases obviously (Fig. 2c). These observations are well correlated with work (Kondrotas et al., 2015), where the model of growth of CZTSe films enriched with Zn is proposed. According to this model, CZTSe crystals grow large and form a compact layer, leaving an
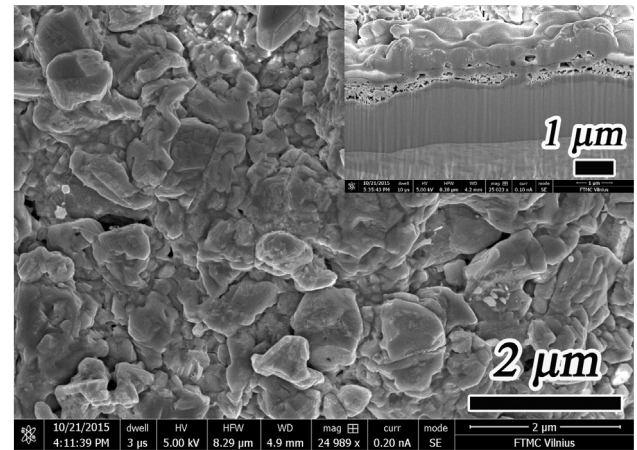

Fig. 3. Top view SEM images of CZTSe films series C after 30 min of selenization at 580 °C. Inset to (*a*) shows the typical cross-sectional image of the CZTSe film series C.

excess of zinc at the surface. The ZnSe crystallites located on the surface of the film can be effectively removed by etching. According to the data of SEM (Fig. 1), the thickness of the CZTSe layer slightly increased as the selenization time increased.

The SEM images show no significant changes to the surface morphology of CZTSe films between 560 and 580 °C (Fig. 3). However, the thickness of the CZTSe layer obtained at 580 °C is 1.2 μm, which is much less, than the thickness of the layer of the CZTSe films obtained at 560 °C.

The X-ray diffraction (XRD) patterns of CZTSe films series A and B obtained by annealing at temperature of 560 °C for three different duration: 10, 20 and 30 min are shown in Fig. 4. In both series, the XRD patterns of the CZTSe films selenized for 10 min reveal the formation of $Cu_2ZnSnSe_4$ (Card No.: 96-722-0527) phase. In the XRD patterns, there

Fig. 2. Top view SEM images of CZTSe films series B obtained at selenization temperature of 560 °C and selenization time of 10 (*a*), 20 (*b*) and 30 (*c*) min with EDX point measurements.
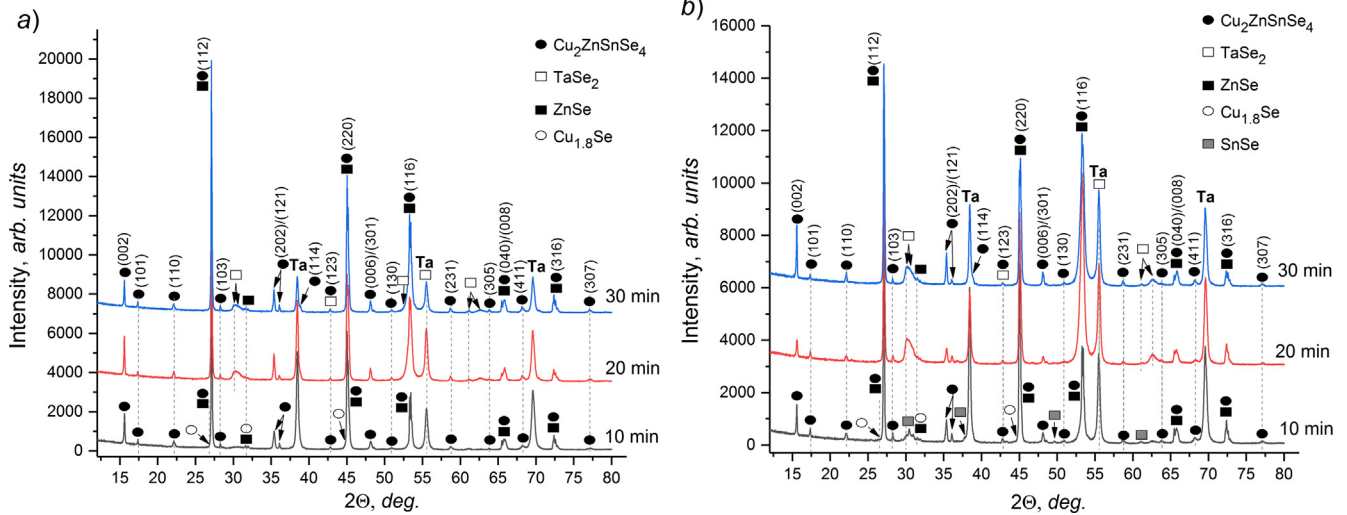
Fig. 4. Typical XRD patterns of CZTSe films series A (*a*) and B (*b*) after 10, 20 and 30 min of selenization at 560 °C.

are also reflections from the Ta substrate and $Cu_{1.8}Se$ (Card No.: 96-900-8067). The compositions of CZTSe films of two series can involve also the ZnSe phase (Card No.: 00-037-1463). The presence of ZnSe phase is quite difficult to rule out due to the closeness of the most intense peaks of this phase with those of $Cu_2ZnSnSe_4$ phase. In addition, in the XRD pattern of CZTSe film series B (Fig. 4b), there are low-intensity reflections of the SnSe phase (Card No.: 96-153-8897). According to Collord et al. (2015) and Vauche (2015), Sn-Se secondary phases are expected in the Cu-poor composition with the ratio Zn/Sn > 1, since this region is actually Zn-rich and Sn-rich. However, detection of the Sn-Se secondary phases by XRD is challenging, as the peaks of this phases are less intense, probably due to small concentrations and non-uniform distribution at the surface (Vauche, 2015). Nevertheless, according to Vauche (2015), the Sn-Se secondary phases are detected quite easily by SEM analysis of the surface, what is consistent with our SEM results (Fig. 2b).

The XRD patterns of CZTSe films series A and B revealed that the peak from the (1 1 2)-plane intensity becomes stronger when selenization time increases, indicating that the film crystallinity gradually gets better. In the XRD patterns of CZTSe films series A the full width at half maximum (FWHM) peak from the (1 1 2)-plane decreases from 0.16 to 0.14 as the selenization time increases. That confirms the improvement in crystallographic structure. In contrast, the FWHM peak from the (1 1 2)-plane decreases (from 0.14 to 0.18) with increasing selenization time in the CZTSe films series B. It is known that the line broadening is a result of small crystallite size and large microdeformations (Δd/d) in the growth direction of the coating.

Moreover, a further increase of selenization time leads to formation of $TaSe_2$ (Card No.: 96-231-0533) phase and to disappearance of $Cu_{1.8}Se$ phase. It should be noted that the SnSe XRD peak intensity increased with the increasing in selenization time up to 20 min and SnSe peak vanished at selenization time of 30 min (Fig. 4b).

The XRD pattern of the CZTSe thin film selenized for 30 min at 580 °C (Fig. 5) reveals the formation of CZTSe phases with $TaSe_2$ and ZnSe secondary phases, which are consistent with results of CZTSe films selenization duration 30 min at 560 °C.

The lattice parameters calculated from the XRD data of CZTSe films depending on time and temperature of selenization are presented in Table 2. As can be seen, the volume of the CZTSe unit cell decreases with the selenization time. The CZTSe films series A and C have larger lattice parameters than the theoretical values. In contrast, the lattice parameters of the CZTSe films series B have lower value than theoretical ones.

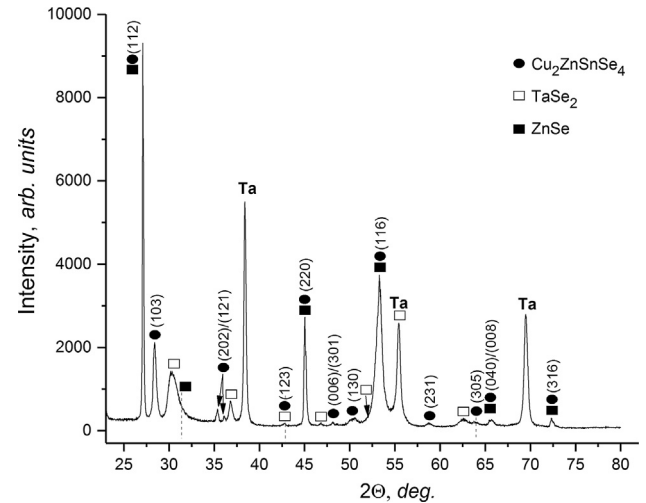It is known that the CZTSe can crystallize into the kesterite or

Fig. 5. Typical XRD patterns of CZTSe film series C after 30 min of selenization at 580 °C.

stannite structure. However, from the results of XRD analysis, it is impossible to determine reliably which of the two structures has been formed. Authors Olekseyuk et al. (2002) showed that the $Cu_2ZnSnSe_4$ single crystal with stannite structure exhibits the lattice parameters: $a = 5.6882$ Å, $c = 11.3378$ Å, and $\eta = 1.0034$. According to (Chen et al., 2009), CZTSe with the kesterite structure must have the somewhat larger lattice parameter and the somewhat smaller tetragonal distortion η ($\eta = c/2a$) compared to the corresponding parameters of the stannite structure. In addition, one more structure that can be formed by the CZTSe alloy is the partially disordered kesterite, which can lead to a volumetric expansion of up to 0.3% (Schorr et al., 2007). Taking into consideration the above-listed structural features of kesterite and stannite and the results of this study, we can conclude that all films crystallized with the formation of the kesterite or partially disordered kesterite structure.

The microstrain (ε) values presented in Table 3 were calculated using the relation (Levandi, 2013):

$$\varepsilon = (c - c_o)/c_o * 100\%, \tag{1}$$

where c is the lattice parameters evaluated from the XRD data and c_o is the bulk lattice parameters.

The increase of the selenization time leads to a decrease of ε values. Such a change of microstrain in crystallite is possible due to come from

Table 2
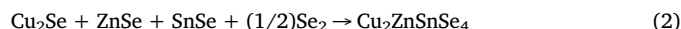The lattice parameters of CZTSe and secondary phases.

Series	Temperature of selenization, °C	Time of selenization, min	The experimental data											
			CZTSe				ZnSe		CuSe		SnSe			
			a, Å	c, Å	V	η	a, Å	V	a, Å	V	a, Å	b, Å	c, Å	V
A	560	10	5.698 ± 0.001	11.352 ± 0.001	368.568	0.996	5.682 ± 0.001	183.444	5.668 ± 0.001	182.091	–	–		
		20	5.697 ± 0.001	11.348 ± 0.002	368.309	0.996	5.666 ± 0.001	181.899	–		–	–		
		30	5.696 ± 0.001	11.347 ± 0.001	368.147	0.996	5.66 ± 0.001	181.321	–		–	–		
B		10	5.695 ± 0.001	11.344 ± 0.001	367.920	0.996	5.661 ± 0.001	181.418	5.724 ± 0.005	187.542	11.828 ± 0.003	4.028 ± 0.002	4.34 ± 0.002	206.771
		20	5.692 ± 0.001	11.333 ± 0.002	367.176	0.996	5.648 ± 0.002	180.171	–		11.817 ± 0.005	4.036 ± 0.003	4.377 ± 0.005	208.754
		30	5.691 ± 0.001	11.327 ± 0.002	366.853	0.995	5.603 ± 0.002	175.898	–		–			
C	580	30	5.699 ± 0.001	11.345 ± 0.002	368.470	0.995	5.656 ± 0.002	180.937	–		-			
The theoretical data			5.697 (JCPDS 96-722-0527)	11.339	368.016	0.995	5.667 (JCPDS 00-037-1463)	181.995	5.729 (JCPDS 96-900-8067)	188.034	11.42 (JCPDS 96-153-8897)	4.19	4.46	213.410

Table 3
The microstrain values (ε, %) for CZTSe films.

Series	Temperature of selenization, °C	Time of selenization, min	CZTSe
A	560	10	0.11
		20	0.08
		30	0.07
B		10	0.04
		20	−0.05
		30	−0.11
C	580	30	0.05

dislocations (mostly), vacancies, thermal expansions and contractions.

Fig. 6a–c show a SIMS depth profile of CZTSe films series A after 10, 20 and 30 min of selenization at 560 °C, respectively. As can be seen from Fig. 6a–c the significant increase of Ta signal around the sputter time of 400/700 sec indicates the start of the CZTSe/Ta interface. It can be seen, that the elements Se, Sn, Zn and Cu to some extent are intermixed in the film and at the film/interface in the CZTSe films obtained at temperature 560 °C within 10 and 20 min. It is observed a gradual increase of the Zn and decrease of the Cu intensity from the near-surface region to the back side of films (Fig. 6a and b). The increase in the intensity of Zn in the absorber layer at the CZTSe/TaSe$_2$ interface can be attributed to residual ZnSe secondary phase formed. In works Arasimowicz (2014) and Vauche (2015) it is reported that zinc partially migrates towards the copper layer directly after electrodeposition of precursors with the layers sequence substrate/Cu/Sn/Zn. In addition, the subsequent low-temperature annealing of precursors leads to the formation of Cu-Zn alloy at the back of the precursor side while the surface of precursor consists of a mixture of Cu-Sn alloy and Sn. Such the bi-layer structure of the precursors indicates a Zn-rich region at the backside of the metal precursors. According to the proposed reaction pathway of CZTSe formation from Cu-Sn-Zn precursors (Eqs. (2) and (3)), binary and/or ternary phases are formed during high-temperature annealing of precursors in selenium vapor, which then are transformed into the main phase Cu$_2$ZnSnSe$_4$.

$$Cu_2Se + ZnSe + SnSe + (1/2)Se_2 \rightarrow Cu_2ZnSnSe_4 \tag{2}$$

$$Cu_2SnSe_3 + ZnSe \rightarrow Cu_2ZnSnSe_4 \tag{3}$$

This indicates that in our case the elements interdiffusion process is incomplete and agrees with the XRD data revealed the coexistence of the ZnSe and the Cu$_2$ZnSnSe$_4$ phases in the CZTSe films annealed within 10 and 20 min. Moreover, this explains the formation of a Zn-rich area on the backside of the CZTSe film, with Zn being the top layer of the precursors. On the other hand, the CZTSe film synthesized within 30 min at 560 °C exhibits more homogeneous mixing of elements throughout the entire film depth (Fig. 6c).

In the middle of the CZTSe film obtained at 560 °C within 30 min (Fig. 6c), the CZTSe phase has been formed. Nevertheless, at the CZTSe/Ta interface an unreacted ZnSe residue is seen. The presence of a signal from Ta in the CZTSe films layer is possibly associated with a small thickness of CZTSe layer (Fig. 3).

Fig. 7 shows spectral reflection curves of the CZTSe films series A obtained during different times selenization at 560 °C. It is observed that the reflection of the CZTSe films was decreased as selenized time increased because of the improving the structure of the CZTSe films and increase of grain size which means increase in the absorption.

The band-gap value of films was evaluated from the measurements of reflectance spectra using the Kubelka-Munk (K-M) theory (Kubelka, 1948). This theory provides the descriptions of diffuse reflectance spectroscopy. The K-M method is based on the following equation:

$$k/s = (1 - R_\infty)^2 / 2 \cdot R_\infty = f(R1), \tag{4}$$

where k – absorption coefficient, s – scattering coefficient, R_∞ is the reflectance and R_1 is the absolute reflectance (K-M function).
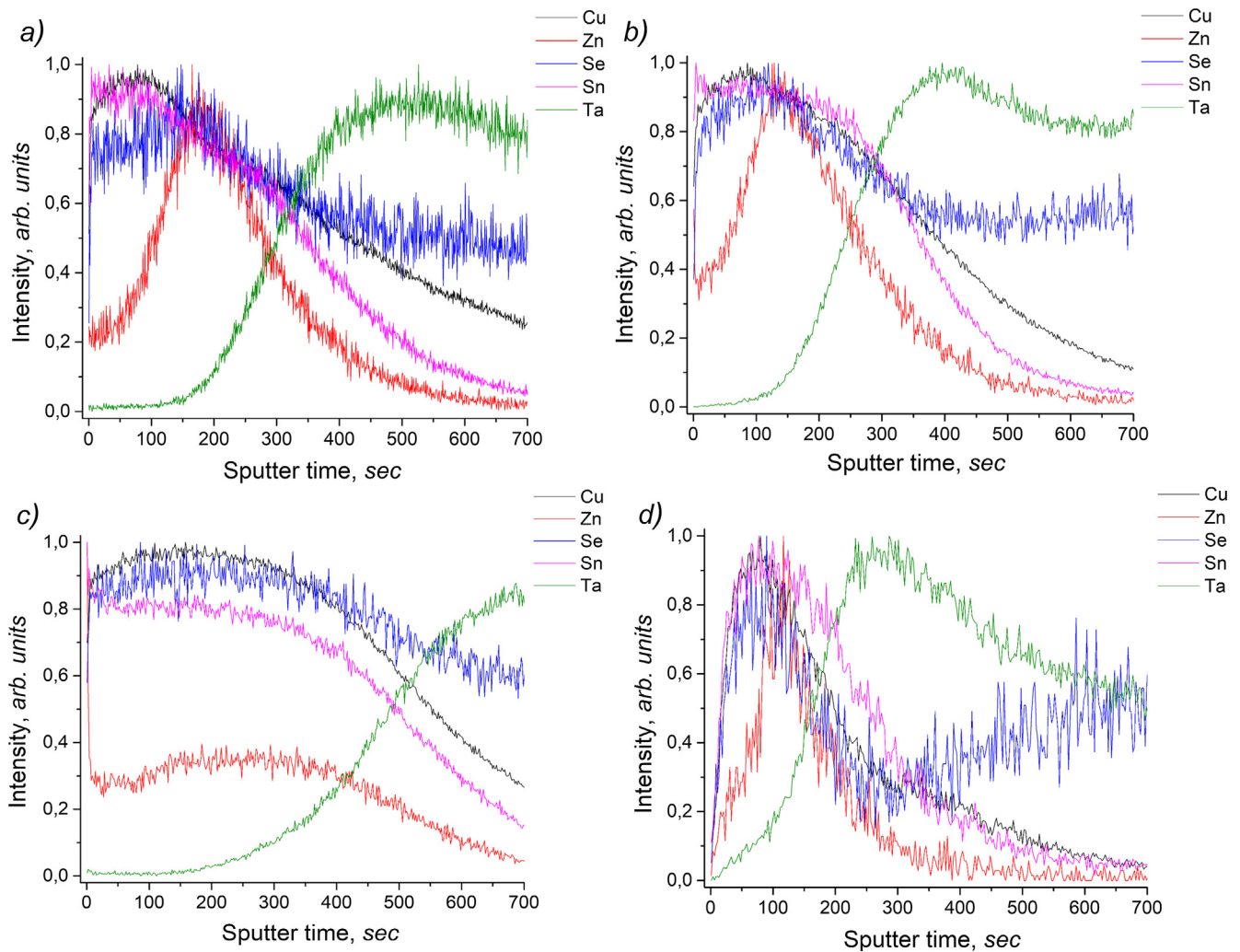
Fig. 6. SIMS depth profiles of CZTSe films series A after 10 (*a*), 20 (*b*) and 30 (*c*) min of selenization at 560 °C and series C (*d*) after 30 min of selenization at 580 °C.
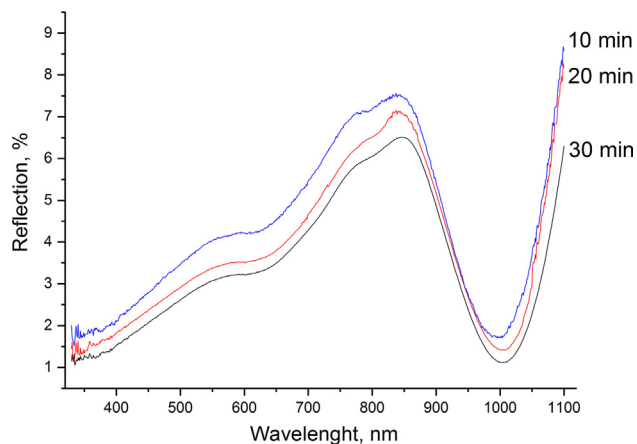

Fig. 7. Reflection spectra of CZTSe films series A after 10, 20 and 30 min of selenization at 560 °C.

Fig. 8a and b show the plots of $[(k/s \cdot h\nu)]^2$ vs $h\nu$ for the CZTSe films series A and C. It was found that the optical band gaps were 1.16, 1.17, 1.19 and 1.22 eV for the films series A after 10, 20 and 30 min of selenization at 560 °C and films series C after 30 min of selenization at 580 °C, respectively.

It should be noticed that E_g of the films increased gradually from 1.16 to 1.19 eV as the selenization time increased from 10 to 30 min.

The increase in E_g is thought to be related with several causes. According to Tuttle et al. (1988) and Babu et al. (2008), the optical band gap of CZTSe thin films decreases slightly with the increase in the Cu/(Zn + Sn) ratio. Another cause of the optical band gap decrease is the percentage of transmittance, which is decreasing with increase in thickness of the film (Kanuru et al., 2014). The third cause is presence of secondary phases in composition of CZTSe thin films.

It can be said that the estimated results are quite close to the theoretical value of band gap for CZTSe. The small difference between the obtained and theoretical values of the optical band gap in our case might be due to a slight difference in the film composition and presence of secondary phases.

4. Conclusions

In this work, the CZTSe thin films were produced onto flexible Ta metal foils by a three-step process and the effect of selenization time and temperature on the microstructure and optical properties of these films was investigated. It is shown that the amount of tin in the composition of CZTSe films decreases with the increasing time and temperature of selenization. Therefore, in order to compensate its loss, it is necessary to use precursors with a slight enrichment of tin. It is established that the CZTSe film selenized at 560 °C for 30 min exhibits the best morphology and crystal structure compared to the CZTSe films which annealed for shorter time. The CZTSe films selenized at temperatures of 560 and 580 °C for 30 min show the same surface
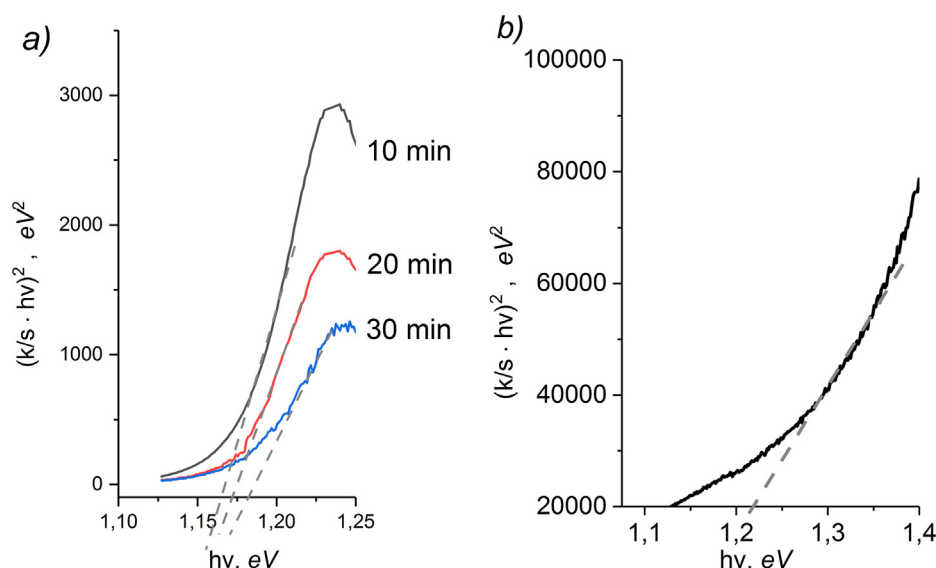
Fig. 8. Dependency $[(k/s \cdot h\nu)]^2$ vs $h\nu$ of the CZTSe films series A (*a*) and C (*b*) and extraction of band gaps via linear extrapolation to zero (dashed lines).

morphology. In both cases, presence of $Cu_2ZnSnSe_4$ basic phase, $TaSe_2$ and ZnSe phases in compositions of the CZTSe films was detected. It is found that the CZTSe films have kesterite or disordered kesterite structure with the lattice parameters close to the theoretical values. Furthermore, the optical band gap of CZTSe films varies in the range of 1.16–1.22 eV, depending on selenization duration and temperature. From above results, it is evident that the phase composition and morphology of CZTSe films can be easily controlled by adjusting the selenization time and temperature. The obtained results for growth of the CZTSe films indicate that the optimal conditions for precursors selenization are temperature 560 °C and time 30 min. In addition, this work demonstrates that it is possible to grow the CZTSe thin films on flexible metal substrates by suggested approach, which can be used for fabrication of solar cells.

Acknowledgments

References

Abermann, S., 2013. Non-vacuum processed next generation thin film photovoltaics: towards marketable efficiency and production of CZTS based solar cells. Sol. Energy 94, 37–70.

Aksu, S., Wang, J.X., Basol, B.M., 2009. Electrodeposition of In-Se and Ga-Se thin films for preparation of CIGS solar cells. Electrochem. Solid State Lett. 12 (5), D33–D35.

Amiri, N.B.M., Postnikov, A., 2012. Secondary phase $Cu_2ZnSnSe_3$ vs. kesterite $Cu_2ZnSnSe_4$: similarities and differences in lattice vibration modes. J. Appl. Phys. 112, 033719.

Arasimowicz, M., 2014. Phase Segregation in $Cu_2ZnSnSe_4$ Thin Films for Photovoltaic Applications: The Effects of Precursor Microstructure and Selenium Activity during Selenization of Electrodeposited Metallic Precursors. Universite Luxembourg, Luxembourg.

Babu, G.S., Kumar, Y.B.K., Bhaskar, P.U., Raja, V.S., 2008. Growth and characterization of co-evaporated $Cu_2ZnSnSe_4$ thin films for photovoltaic applications. J. Phys. D: Appl. Phys. 41, 205305.

Bojic, M., Radulovic, J., Rankovic, V., Nikolic, D., Bojic, L., Skerlic, J., 2016. Flexible thin-film solar photovoltaics: research and application. Int. J. Eng. 37–40.

Chen, S., Gong, X.G., Walsh, A., Wei, S.H., 2009. Crystal and electronic band structure of Cu_2ZnSnX_4 (X = S and Se) photovoltaic absorbers: first-principles insights. Appl. Phys. Lett. 94, 041903.

Collord, A.D., Xin, H., Hillhouse, H.W., 2015. Combinatorial exploration of the effects of intrinsic and extrinsic defects in $Cu_2ZnSn(S, Se)_4$. IEEE J. Photovoltaics 5 (1), 288–298.

Das, S., Mandal, K.C., Bhattacharya, R.N., 2016. Earth-abundant $Cu_2ZnSn(S, Se)_4$ (CZTSSe) Solar Cells. In: Paranthaman, M.P., Wong-Ng, W., Bhattacharya, R.N. (Eds.), Semiconductor Materials for Solar Photovoltaic Cells, Switzerland, pp. 25–74.

Deligianni, H., Ahmed, S., Romankiw, L.T., 2011. The next frontier: electrodeposition for solar cell fabrication. J. Electrochem. Soc. Interface 20 (2), 47–53.

Fairbrother, A., Fontane, X., Izquierdo-Roca, V., Placidi, M., Sylla, D., Espindola-Rodriguez, M., Lopez-Marino, S., Pulgarín, F.A., Vigil-Galán, O., Pérez-Rodríguez, A., Saucedo, E., 2014. Secondary phase formation in Zn-rich $Cu_2ZnSnSe_4$-based solar cells annealed in low pressure and temperature conditions. Prog. Photovolt: Res. Appl. 22, 479–487.

Fella, C.M., Uh, A.R., Romanyuk, Y.E., Tiwari, A.N., 2012. $Cu_2ZnSnSe_4$ absorbers processed from solution deposited metal salt precursors under different selenization conditions. Phys. Status Solidi A 209 (6), 1043–1048.

Fella, C.M., Uhl, A.R., Hammond, C., Hermans, I., Romanyuk, Y.E., Tiwari, A.N., 2013. Formation mechanism of $Cu_2ZnSnSe_4$ absorber layers during selenization of solution deposited metal precursors. J. Alloy. Compd. 567, 102–106.

Green, M.A., 2009. Estimates of Te and In prices from direct mining of known ores. Prog. Photovolt. Res. Appl. 17, 347–359.

Green, M.A., Hishikawa, Y., Dunlop, E.D., Levi, D.H., Hohl-Ebinger, J., Ho-Baillie, A.W.Y., 2017. Solar cell efficiency tables (Version 51). Prog. Photovolt. Res. Appl. 26, 3–13.

Gremenok, V.F., Juskenas, R., Bashkirov, S.A., Tyukhov, I.I., Kim, W.Y., Chai, S.H., 2016. $Cu_2ZnSnSe_4$ thin films on flexible substrates for solar cells application. Res. Agric. Electric Eng. 4 (2), 39–42.

Gremenok, V.F., Juskenas, R., Petlitskaya, T.V., Stanchik, A.V., Bashkirov, S.A., Giraitis, R., Selskis, A., Pyatlitski, A.N., Solodukha, V.A., Berthold, C., Nickel, K., 2017. Growth and properties of $Cu_2ZnSnSe_4$ films on flexible metallic substrates. In: Proceedings of the 33rd European Photovoltaic Solar Energy Conference and Exhibition, pp. 1081–1084.

Guo, L., Zhu, Y., Gunawan, O., Gokmen, T., Deline, V.R., Ahmed, S., Romankiw, L.T., Deligianni, H., 2014. Electrodeposited $Cu_2ZnSnSe_4$ thin film solar cell with 7% power conversion efficiency. Prog. Photovolt. Res. Appl. 22 (1), 58–68.

Hartnauer, S., Körbel, S., Marques, M.A.L., Botti, S., Pistor, P., Scheer, R., 2016. Research update: stable single-phase Zn-rich $Cu_2ZnSnSe_4$ through In doping. APL Mater. 4, 070701.

Jayawardena, K.I., Rozanski, L.J., Mills, C.A., Beliatis, M.J., Nismy, N.A., Silva, S.R.P., 2013. Inorganics-in-organics: recent developments and outlook for 4G polymer solar cells. Nanoscale 5, 8411–8427.

Jiang, F., Ikeda, S., Harada, T., Matsumura, M., 2013. Pure Sulfide Cu_2ZnSnS_4 thin film solar cells fabricated by preheating an electrodeposited metallic stack. Adv. Energy Mater. 4, 1301381.

Just, J., Sutter-Fella, C.M., Lutzenkirchen-Hecht, D., Frahm, R., Schorr, S., Unold, T., 2016. Secondary phases and their influence on the composition of the kesterite phase in CZTS and CZTSe thin films. Phys. Chem. Chem. Phys. 18, 15988–15994.

Kaigawa, R., Hashimoto, Sh., Irago, T., Klenk, R., 2015. Direct preparation of $Cu_2ZnSnSe_4$ films by microwave irradiation and its dependence on the Sn/(Sn + Zn) ratio. Jpn. J. Appl. Phys. 54, 08KC02.

Kanuru, C.S., Shekar, G.L., Krishnamurthy, L., Gopal, R., Urs, K., 2014. Surface morphological studies of solar absorber layer Cu_2ZnSnS_4 (CZTS) thin films by non-vacuum deposition methods. J. Nano- Electronic Phys. 6 (2), 02004.

Kessler, F., Herrmann, D., Powalla, M., 2005. Approaches to flexible CIGS thin-film solar cells. Thin Solid Films 480–481, 491–498.

Kessler, F., Rudmann, D., 2004. Technological aspects of flexible CIGS solar cells and modules. Sol. Energy 77, 685–695.

Khalil, M.I., Bernasconi, R., Pedrazzetti, L., Lucotti, A., Donne, L.A., Binetti, S., Magagnin, L., 2017. Co-electrodeposition of metallic precursors for the fabrication of CZTSe thin films solar cells on flexible Mo foil. J. Electrochem. Soc. 164 (6), D302–D306.

Kim, K.M., Kim, Sh., Tampo, H., Shibata, H., Matsubara, K., Niki, S., 2016. Effect of pre-annealing on $Cu_2ZnSnSe_4$ thin-film solar cells prepared from stacked Zn/Cu/Sn metal precursors. Mater. Lett. 176, 78–82.

Klochko, N.P., Khrypunov, G.S., Volkova, N.D., Kopach, V.R., Momotenko, A.V., Lubov, V.N., 2014. Structure and properties of electrodeposited films and film stacks for precursors of chalcopyrite and kesterite solar cells. Semiconductors 48 (4), 521–530.

Kondrotas, R., Juskenas, R., Naujokaitis, A., Selskis, A., Giraitis, R., Mockus, Z., Kanapeckaite, S., Niaura, G., Xie, H., Sanchez, Y., Saucedo, E., 2015. Characterization of $Cu_2ZnSnSe_4$ solar cells prepared from electrochemically co-deposited Cu–Zn–Sn alloy. Sol. Energy Mater. Sol. Cells 132, 21–28.

Kubelka, P., 1948. New contributions to the optics of intensely light-scattering materials. Part I. J. Opt. Soc. Am. 38 1067–1067.

Lee, Y.S., Gershon, T., Gunawan, O., Todorov, T.K., Gokmen, T., Virgus, Y., Guha, S., 2014. $Cu_2ZnSnSe_4$ thin-film solar cells by thermal coevaporation with 11.6% efficiency and improved minority carrier diffusion length. Adv. Energy Mater 1401372.

Levandi, T., 2013. Comparative Study of Cereal Varieties by Analytical Separation Methods and Chemometrics. Tallinn University of Technology Faculty of Science, Eesti.

Lopez-Marino, S., Sancheza, Y., Espindola-Rodriguez, M., Alcobe, X., Xie, H., Neuschitzer, M., Becerril, I., Giraldo, S., Dimitrievska, M., Placidi, M., Fourdrinier, L., Izquierdo-Roca, V., Perez-Rodrigueza, A., Saucedo, E., 2016. Alkali doping strategies for flexible and light-weight $Cu_2ZnSnSe_4$ solar cells. J. Mater. Chem. A 1–16.

Luck, I., 2014. Competitiveness of CIGS technology in the light of recent PV developments - Part I: the state of the art in CIGS production. Photovolt. Int. 69–72.

Lutterotti, L., Matthies, S., Wenk, H.R., 1999. MAUD (Material Analysis Using Diffraction): a user friendly Java program for Rietveld Texture Analysis and more. In: Proceedings of the 12th International Conference on Textures of Materials (ICOTOM-12), vol. 1, p. 1599.

Mangan, T.C., McCandless, B.E., Dobson, K.D., Birkmire, R.W., 2015. Thermochemical and kinetic aspects of $Cu_2ZnSn(S, Se)_4$ thin film growth by reacting Cu-Zn-Sn precursors in H_2S and H_2Se. J. Appl. Phys. 118, 065303.

Marquez-Prieto, J., Yakushev, M.V., Forbes, I., Krustok, J., Edwards, P.R., Zhivulko, V.D., Borodavchenko, O.M., Mudryi, A.V., Dimitrievska, M., Izquerdo-Roca, V., Pearsall, N.M., Martin, R.W., 2016. Impact of the selenization temperature on the structural and optical properties of CZTSe absorbers. Sol. Energy Mater. Sol. Cells 152, 42–50.

Moskowitz, P.D., Fthenakis, V.M., 1990. Toxic materials released from photovoltaic modules during fires: health risks. Solar Cells 29 (1), 63–71.

Olekseyuk, I.D., Gulay, L.D., Dydchak, I.V., Piskach, L.V., Parasyuk, O.V., Marchuk, O.V., 2002. Single crystal preparation and crystal structure of the Cu_2Zn/Cd, $Hg/SnSe4$ compounds. J. Alloy. Compd. 340, 141–145.

Otte, K., Makhova, L., Braun, A., Konovalov, I., 2006. Flexible $Cu(In, Ga)Se_2$ thin-film solar cells for space application. Thin Solid Films 511–512, 613–622.

Pagliaro, M., Palmisano, G., Ciriminna, R., 2008. Flexible Solar Cells. Wiley-VCH, Weinheim, pp. 1–30.

Redinger, A., Siebentritt, S., 2010. Coevaporation of $Cu_2ZnSnSe_4$ thin films. Appl. Phys. Lett. 97, 092111.

Rietveld, H.M., 1969. A profile refinement method for nuclear and magnetic structures. J. Appl. Cryst. 2, 65–71.

Salome, P.M.P., Fernandes, P.A., Leita, J.P., Sousa, M.G., Teixeira, J.P., Cunha, A.F., 2014. Secondary crystalline phases identification in $Cu_2ZnSnSe_4$ thin films: contributions from Raman scattering and photoluminescence. J. Mater. Sci. 49, 7425–7436.

Schorr, S., 2007. Structural aspects of adamantine like multinary chalcogenides. Thin Solid Films 515 (15), 5985–5991.

Stanchik, A.V., Gremenok, V.F., Bashkirov, S.A., Tivanov, M.S., Juskenas, R.L., Novikov, G.F., Giraitis, R., Saad, A.M., 2018. Microstructure and Raman scattering of $Cu_2ZnSnSe_4$ thin films deposited onto flexible metal substrates. Semiconductors 52 (2), 227–232.

Temgoua, S., Bodeux, R., Naghavi, N., Delbos, S., 2014. Effects of $SnSe_2$ secondary phases on the efficiency of $Cu_2ZnSn(S_x, S_{e1-x})_4$ based solar cells. Thin Solid Films 582, 215–219.

Tuttle, J., Albin, D., Goral, J., Kennedy, C., Noufi, R., 1988. Effects of composition and substrate temperature on the electro-optical properties of thin film $CuInSe_2$ and $CuGaSe_2$. Sol. Cells 24, 67–79.

Vauche, L., 2015. Process Development and Scale-Up for Low-Cost High-Efficiency Kesterite Thin Film Photovoltaics. Micro and Nanotechnologies/Microelectronics. Universite d'Aix Marseille, Franz.

Xie, H., Dimitrievska, M., Fontane, X., Sanchez, Y., Lopez, S., Izquierdo, V., Bermudez, V., Perez, A., Saucedo, E., 2015. Formation and impact of secondary phases in Cu-poor Zn-rich $Cu_2ZnSn(S_{1-y}Se_y)_4$ ($0 \leq y \leq 1$) based solar cells. Sol. Energy Mater. Sol. Cells 140, 289–298.

Yao, L., Ao, J., Jeng, M., Bi, J., Gao, S., Sun, G., He, Q., Zhou, Z., Sun, Y., Chang, L., 2017. A CZTSe solar cell with 8.2% power conversion efficiency fabricated using electro-deposited Cu/Sn/Zn precursor and a three-step selenization process at low Se pressure. Sol. Energy Mater. Sol. Cells 59, 318–324.